THE JOURNAL OF BIOLOGICAL CHEMISTRY VOL. 281, NO. 24, pp. 16462–16472, June 16, 2006

On the Mechanism of Nucleosome Assembly by Histone Chaperone NAP1*[S]

Received for publication, October 26, 2005, and in revised form, February 27, 2006 Published, JBC Papers in Press, March 12, 2006, DOI 10.1074/jbc.M511619200

Jacek Mazurkiewicz, J. Felix Kepert, and Karsten Rippe[1]

From the Molecular Biophysics Group, Kirchhoff-Institut für Physik, Ruprecht-Karls-Universität Heidelberg, Im Neuenheimer Feld 227, D-69120 Heidelberg, Germany

The process of mononucleosome assembly mediated by histone chaperone NAP1 was investigated using DNA fragments 146 and 207 bp in length containing the *Lytechinus variegatus* 5 S rDNA nucleosome positioning sequence. A quantitative description was derived using gel electrophoresis and fluorescent anisotropy data. First, NAP1-bound H3·H4 was released forming a DNA-histone tetramer complex with a time constant of $k_1 = (2.5 \pm 0.7) \cdot 10^4\ \mathrm{M}^{-1}\ \mathrm{s}^{-1}$. The tetrasome was converted quickly ($k_2 = (4.1 \pm 3.5) \cdot 10^5\ \mathrm{M}^{-1}\ \mathrm{s}^{-1}$), by the addition of a single H2A·H2B dimer, into a "hexasome," *i.e.* a nucleosome lacking one H2A·H2B dimer. From this intermediate a nucleosome was formed by the addition of a second H2A·H2B dimer with an average rate constant $k_3 = (6.6 \pm 1.4) \cdot 10^3\ \mathrm{M}^{-1}\ \mathrm{s}^{-1}$. For the back-reaction, significant differences were observed between the 146- and 207-bp DNA upon substitution of the canonical H2A histone with H2A.Z. The distinct nucleosome/hexasome ratios were reflected in the corresponding equilibrium dissociation constants and revealed some differences in nucleosome stability. In a fourth reaction, NAP1 mediated the binding of linker histone H1 to the nucleosome, completing the chromatosome structure with $k_4 = (7.7 \pm 3.7) \cdot 10^3\ \mathrm{M}^{-1}\ \mathrm{s}^{-1}$. The activity of the chromatin remodeling complex ACF did not increase the kinetics of the mononucleosome assembly process.

The repeating building block of chromatin is the nucleosome, a nucleoprotein complex consisting of two each of histones H2A, H2B, H3, and H4 wrapped around 146/147 bp of DNA (1). Several studies have focused on the mechanism by which these entities are assembled and how a defined chromatin structure is established (2–10). *In vivo* chromatin assembly is mostly coupled to DNA replication (11), but recent investigations have pointed out the importance of replication-independent deposition of variant histones such as H2A.Z and H3.3. This process appears to be relevant in the formation of chromatin with differential transcriptional activity (12–16). Assembly of nucleosomes seems to be closely linked to the activity of ATP-dependent chromatin remodeling machineries, required for the formation of evenly spaced nucleosome arrays, which are characteristic for the native chromatin conformation (17).

Simple mixing of histones and DNA leads mainly to large, insoluble aggregates (18, 19). Accordingly, the transfer of histones to DNA in the cell is carried out by histone chaperones such as the heterotrimeric chromatin assembly factor 1 (CAF1) (20), N1/N2 (21, 22), nucleoplasmin (23–25), HIRA (26, 27), and nucleosome assembly protein 1 (NAP1)[2] (28, 29). Per definition, all share the capability of binding histones and releasing them to DNA or other targets, but they differ with respect to *in vivo* functions and the preferred histone interaction partner. The histone chaperone NAP1 studied here is involved in the shuttling of newly synthesized histone H2A·H2B dimers from the cytoplasm to the nucleus and the deposition of histones onto the DNA (3, 17, 30). In addition, NAP1 has been reported to play a role in chromatin remodeling and the incorporation of variant histones into chromatin (29, 31–33). The structure of a yeast NAP1 dimer has been determined recently by x-ray crystallography (34). Although NAP1 is generally regarded as a carrier for the H2A·H2B dimer, it interacts with similar affinity with H3·H4 *in vitro* (32, 35, 36) and has been used as sole histone carrier for chromatin reconstitution with the chromatin assembly/remodeling factor ACF (37). Furthermore, recent results report the interaction of NAP1 with linker histones (38, 39).

During nucleosome assembly the histone transfer seems to follow a defined scheme. First, a tetrasome consisting of an $(H3{\cdot}H4)_2$ tetramer is formed on the DNA followed by the addition of two H2A·H2B dimers. In a final step the linker histone H1 is added to the core nucleosome yielding a complex, which is referred to here to as the chromatosome. This stepwise assembly mechanism has been shown for chromatin formation *in vivo* (10, 40–44) as well as for a wide range of *in vitro* assays (45). These include reconstitution reactions with nuclear extracts (46, 47), purified or recombinant factors at physiological salt concentrations (48–50), as well as protocols that utilize salt gradients (51–54). Hence, this assembly order appears to be governed by the intrinsic physical properties of the histones themselves. Accordingly, nucleosomes can be formed with predeposited H3·H4 tetrasomes but assemble only inefficiently on H2A·H2B-DNA complexes (49, 53, 55).

In this study NAP1 was used in combination with DNA templates of 146 and 207 bp length, recombinant core histones, and linker histone H1 as a minimal system to study the mechanism of mononucleosome assembly mediated by a histone chaperone under well defined conditions and at physiological ionic strength. It is shown that NAP1-guided assembly includes an additional intermediate step, as after tetrasome deposition hexasomes are formed, which then maturate into complete nucleosomes. Furthermore, NAP1 assembles H2A.Z-containing nucleosomes mechanistically similar to canonical ones. According to our results, formation of mononucleosomes by NAP1 is not influenced by the energy-dependent activity of chromatin remodeling factors like ACF. Based on these findings and the results of a preceding paper (39), we propose a model in which assembly of nucleosomes up to the level of chromatin is governed by affinity differences of histones between chaperones and binding sites on DNA or (sub)nucleosomal complexes.

* This work was supported by the Volkswagen Foundation "Junior Research Groups at German Universities" program. The costs of publication of this article were defrayed in part by the payment of page charges. This article must therefore be hereby marked "*advertisement*" in accordance with 18 U.S.C. Section 1734 solely to indicate this fact.

[S] The on-line version of this article (available at http://www.jbc.org) contains supplemental Figs. S1–S4.

[1] To whom correspondence should be addressed. Tel.: 49-6221-549270; Fax: 49-6221-549112; E-mail: Karsten.Rippe@kip.uni-heidelberg.de.

[2] The abbreviations used are: NAP1, nucleosome assembly protein 1; ACF, ATP-utilizing chromatin assembly and remodeling factor; H1, linker histone H1; EMSA, electrophoretic mobility shift assay; DNA_{207}/DNA_{146}, DNA fragments of 207/146 bp with the *L. variegatus* 5 S rDNA nucleosome positioning sequence.

EXPERIMENTAL PROCEDURES

Preparation of Proteins—N-terminally His-tagged yeast NAP1 was overexpressed and purified from *Escherichia coli* as described elsewhere (36). Recombinant histone octamer with either canonical H2A or H2A.Z was purified using established protocols (56, 57). Site-specific labeling of histone complexes with Alexa Fluor 488 or 633 C5 maleimide (Molecular Probes Europe BV, Leiden, Netherlands) was performed as described previously using plasmids containing H2A R12C, H2A.Z K5C, H3 C110A, and H4 K5C to obtain Alexa 488-labeled $H2A^f$, $H2A.Z^f$, and $H4^f$ as well as Alexa 633-labeled $H2A^r$ histone complexes (36, 58). The H2A.Z K5C vector was derived from the H2A.Z overexpression vector (14) using the QuikChange mutagenesis kit (Stratagene, La Jolla, CA). Alexa 488-labeled H1 ($H1^f$) was prepared as described previously (39). Labeling efficiency and purification were assessed by absorbance spectroscopy and SDS-PAGE.

Preparation of Nucleic Acids—DNA fragments of 146 bp (DNA_{146}) or 207 bp (DNA_{207}) containing the *Lytechinus variegatus* rDNA sequence were prepared by restriction enzyme digestion (EcoRV or RsaI) with subsequent gel purification from the template pTJR2 (59) or p5S207-12 (60). The *bona fide* random DNA fragment was amplified by PCR from plasmid pET3A using the primer I (CAT ACC GCC AGT TGT TTA CCC) and primer II (GGT CAC TGA TGC CTC CGT) for the 146-bp fragment or primer I and primer III (CAG AAG CCA GAC ATT AAC GCT TC) for the 207-bp fragment. The products were isolated by gel purification.

Gel Electrophoretic Analysis of NAP1-mediated Nucleosome Assembly—For gel electrophoretic analysis, mixtures of NAP1/histone octamer (800/100 nM) and DNA_{207} or DNA_{146} (each 100 nM) were prepared in assembly buffer (10 mM Tris-HCl, pH 7.5, 150 mM KCl, 0.5 mM dithiothreitol, 2 mM $MgCl_2$ and 0.05% Brij-35 (Pierce Biotechnology, Rockford, IL)). In experiments with H1 or ACF (1 ACF complex: 50 histone octamers, reaction supplemented with either 1 mM ATP or CTP) a decreased salt concentration of 75 mM KCl was used. Chromatosome assembly was studied by the addition of preincubated 150 nM $H1^f$ and 300 nM NAP1. The increased ratio of H1 to histone octamer (1.5:1) was chosen to shift the equilibrium more toward chromatosome formation. The samples were incubated at 25 °C for the times indicated prior to loading on a 1% Tris borate-EDTA (Figs. 1, *E* and *F*, 2*C*, 5, and 6 and supplemental Figs. S1–S4) or Tris acetate-EDTA-agarose gel (Figs. 1, *A* and *B*, and 3). Equivalent results were obtained, with Tris acetate-EDTA providing a slightly better separation of species on the 207-bp DNA. The distribution of species was also analyzed by native PAGE using 5.5% (29:1) acrylamide-bisacrylamide gels, which allowed a separation of complexes at different positions on the DNA. Gels were run at approx. 5 V/cm in 0.3× Tris borate-EDTA at 4 °C for 12 h. Bands were visualized by ethidium bromide (EtBr) fluorescence after staining or by recording the Alexa 488 signal of the histone label. Quantification was conducted using ImageQuant software (Amersham Biosciences). For the evaluation of the EtBr signal the amount of free DNA in equilibrium at the end of the time course (typically 10–15%) was determined and used to calculate the amount of histone-DNA complexes from the fraction of bound DNA. The resulting values were used to derive the amount of the different histone-DNA species at the other time points. The time lag in the EMSA experiments between loading the samples on the gel and the stop point of the ongoing assembly reaction was determined to be 200 s. This value was derived from a comparison with the fluorescence anisotropy data as well as from using it as a free parameter when fitting the gel data to the models given in Equations 1–4. Least-squares fitting of kinetic rate constants was performed with the software package GEPASI, which automatically derives differential equations for a given model (61).

Fluorescence Anisotropy Measurements—Fluorescence anisotropy experiments were conducted on a Jasco FP-6300 spectrofluorometer (Jasco, Tokyo, Japan). Histone/NAP1 samples with Alexa-labeled $H4^f$ or $H2A^f$ in assembly buffer were excited at 496 nm, and emission was monitored at 513 nm. $H4^f$ was used for tetrasome assembly and $H2A^f$ for nucleosome assembly. Anisotropy data acquisition and analysis were conducted essentially as described previously (62). The assembly reaction was started by the addition of DNA_{207} or DNA_{146} to a final concentration of 100 nM duplex. Upon transfer of histones from NAP1 to the DNA, the total fluorescence intensity increased, as given by the quenching factor, q. The fraction of histone $H2A^f$ or $H4^f$ bound to DNA at equilibrium, θ_{eq}, was determined in the EMSA experiments from the amount of free DNA and assigned to the fraction of H2A or H4 bound to DNA when the anisotropy signal reached a plateau. The fraction of DNA-bound histone θ in dependence of assembly time t was calculated according to $\theta(t) = (r - r_{NAP1\text{-}H})/[(r - r_{NAP1\text{-}H}) + q \cdot (r_{DNA\text{-}H} - r)]$, where r is the measured anisotropy, $r_{NAP1\text{-}H}$ the anisotropy of the NAP1-histone complex, and $r_{DNA\text{-}H}$ the anisotropy of the DNA-histone complex (63). From the analysis of the data the following values were obtained: (i) octamer formation with DNA_{146}: $\theta_{eq} = 0.63$, $q = 1.25$, $r_{NAP1\text{-}H} = 0.145$ (NAP1-$H2A^f$ complex), $r_{DNA\text{-}H}$ (DNA-$H2A^f$ complex) = 0.098; (ii) octamer formation with DNA_{207}: $\theta_{eq} = 0.72$, $q = 1.48$, $r_{NAP1\text{-}H} = 0.152$ (NAP1-$H2A^f$ complex), $r_{DNA\text{-}H} = 0.086$ (DNA-$H2A^f$ complex); (iii) tetrasome formation with DNA_{207}: $\theta_{eq} = 0.33$, $q = 1.22$, $r_{NAP1\text{-}H} = 0.188$ (NAP1-$H4^f$ complex), $r_{DNA\text{-}H} = 0.139$ (DNA-$H4^f$ complex).

RESULTS AND DISCUSSION

NAP1-mediated Mononucleosome Assembly Proceeds via a Hexasome Intermediate—To investigate the kinetics of nucleosome assembly by histone chaperone NAP1, products and intermediates of the reaction were analyzed on agarose gels (Fig. 1). For this purpose NAP1 and the histone octamer were mixed in a stoichiometric ratio of one histone per NAP1 monomer, which was determined previously as the optimal ratio for complex formation (35, 36). Fractions of this premix were then allowed to react for the indicated times with the 207-bp (DNA_{207}) or 146-bp (DNA_{146}) rDNA fragment, in an equimolar ratio between histone octamers and DNA, and analyzed on agarose gels (Fig. 1). Products were detected via staining of the DNA with EtBr (Fig. 1, *A* and *E*) or by recording the fluorescence of Alexa 488-maleimide-labeled H2A ($H2A^f$) of the same gel (Fig. 1, *B* and *F*). With the Alexa 488 signal three bands were identified, which represent the slow moving $NAP1_2$-($H2A^f$·H2B) complex (36, 39) and two DNA-histone particles (Fig. 1, *B* and *F*). With EtBr staining of the gels (Fig. 1, *A* and *E*) the "complete" nucleosome band was identified from a comparison of the migration behavior with salt-reconstituted nucleosomes (see also Fig. 3*C* and supplemental Fig. S1A). The second species running below the nucleosome was assigned to a hexasome, *e.g.* a subnucleosomal particle, in which only one H2A·H2B dimer is present. Per definition such a complex displays a 50% decreased ratio between histone $H2A^f$ fluorescence and EtBr staining compared with the complete nucleosome. In agreement with this expectation, quantification of the Alexa 488 to EtBr signal showed a ratio of 1.8 ± 0.3 for the normalized $H2A^f$ fluorescence intensity of the nucleosome band to that of the hexasome (Fig. 1, *C* and *G*).

The formation of hexasome and nucleosome particles on both DNAs was quantified by averaging the results from numerous gels. Compared with the DNA_{207} template the abundance of hexasomes increased sig-

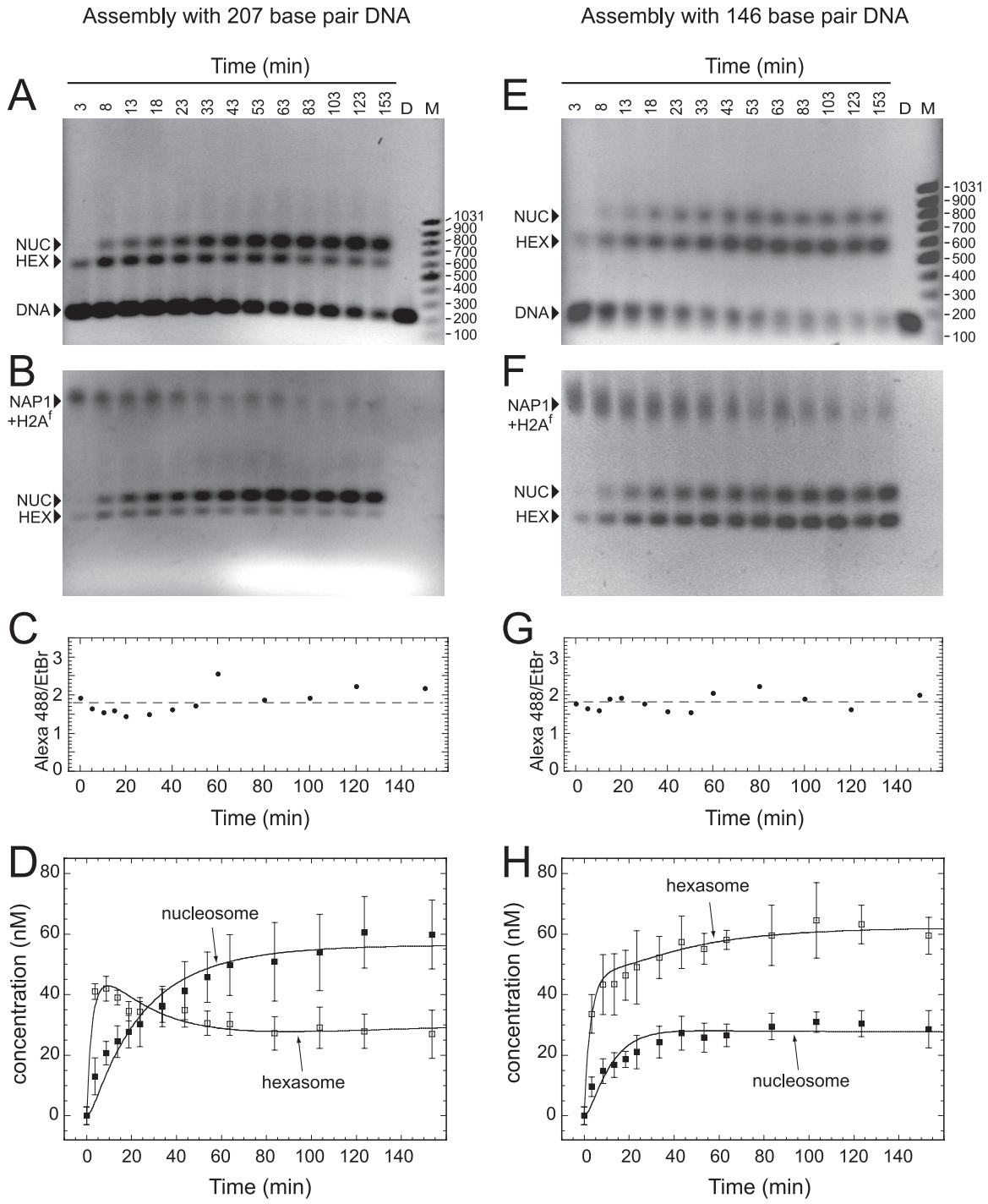

FIGURE 1. **Time course of NAP1-mediated mononucleosome assembly analyzed by agarose gel electrophoresis.** Positions of the $NAP1_2$-($H2A^f$·H2B) complex (*NAP1*+*H2A*^{f}), the nucleosome (*NUC*), the hexasome (*HEX*), and the free DNA (*DNA*) are labeled. *Lane D* contains only DNA_{207} or DNA_{146}, and *lane M* is a 100-bp DNA length standard. On the *left side* (*A–D*) the assembly on the DNA_{207} fragment is analyzed. The *right side* (*E–H*) shows the assembly on DNA_{146}. *A* and *E*, visualization of DNA-containing bands by EtBr staining. *B* and *F*, fluorescence signal of Alexa 488-labeled H2A (*H2A*^{f}) of the gels shown in *panels A* and *E*. *C* and *G*, ratio of the $H2A^f$ (*Alexa 488*) to DNA (*EtBr*) fluorescence. The ratio was normalized to the value of 1 for the putative hexasome band. Thus, a value of 2 is expected for the nucleosome if the hexasome bands represent a species that indeed carries one fluorophore. The average of the determined ratio was 1.83 ± 0.30 (*C*, DNA_{207}) and 1.81 ± 0.20 (*G*, DNA_{146}), demonstrating that the assignment of nucleosome and hexasome is correct. *D*, for quantification of the kinetics, seven time courses with DNA_{207} were averaged, and the resulting fractions of nucleosomes (■) and hexasomes (□) are shown. The *lines* represent a least-squares fit with the model given in Equations 1.1–3.1 and the parameters listed in Table 1. *H*, quantification of six time courses with DNA_{146}. The analysis was conducted as described in *D*.

nificantly with DNA_{146} (Fig. 1, *D* and *H*), and in equilibrium the hexasome band was about twice as prominent as the nucleosomal band. With both DNAs a significant fraction of H2A·H2B remained bound to NAP1, as not all hexasomes maturated to full nucleosomes in equilibrium. However, if more $NAP1_2$-(H2A·H2B) complexes or free H2A·H2B were added, all subnucleosomal particles converted into nucleosomes (data not shown).

The formation of a relatively stable hexameric complex during nucleosome assembly as well as during the NAP1-mediated disintegration reaction (31, 39) appears rather surprising, because the two

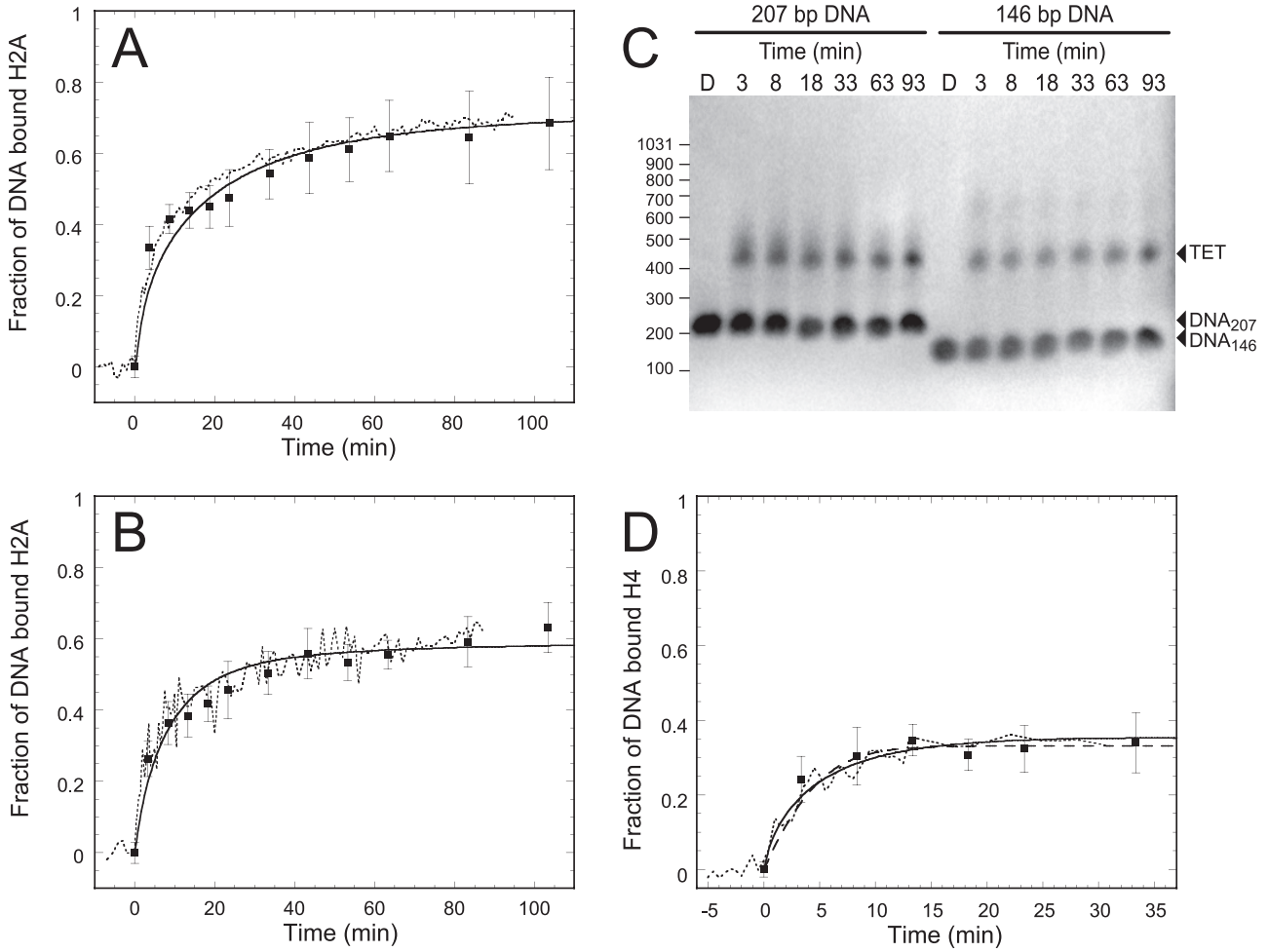

FIGURE 2. **Comparison of assembly kinetics assessed by fluorescence anisotropy and EMSA.** *A*, the assembly reactions were performed with fluorescent $H2A^f$ and DNA_{207}. The measured anisotropy change was converted into the fraction of DNA-bound H2A (*dotted line*). The *solid line* is the fit to the gel electrophoresis data for DNA_{207} (see Fig. 1), where the amount of DNA-bound H2A (■) is given by the concentration of nucleosome and hexasome. *B*, same as in *A* but with DNA_{146}. *C*, gel electrophoretic analysis of the NAP1-mediated assembly of tetrasomes. The assembly kinetics of a solution containing 200 nM recombinant H3·H4 complexed with 400 nM NAP1 were investigated with either DNA_{207} or DNA_{146} at a concentration of 100 nM. The reaction reaches equilibrium quickly, and on average 30–35% of the DNA is complexed into tetrasomes. *D*, quantification of tetrasome assembly kinetics. Fluorescence anisotropy measurements with $H4^f$ and DNA_{207} (*dotted line*) were analyzed as described for *A* and are plotted with the agarose gel electrophoresis data (■). Fits of the anisotropy data to Equations 1.1a and 1.1b are represented by the *solid* and *dashed line*, respectively. The resulting values for the kinetic rate constants were $k_1 = k'_1 \approx k_{1.1}$ $(1.3 \pm 0.4) \cdot 10^4\ M^{-1}\ s^{-1}$ and $k_{-1.2} = 8.7 \pm 2.6 \cdot 10^3\ M^{-1}\ s^{-1}$, which corresponds to $k'_{-1} \approx k'_{-1.2} = 1.8 \pm 0.1 \cdot 10^{-3}\ s^{-1}$.

H2A·H2B dimers adopt symmetric positions within the nucleosome. A possible explanation would be differences between the hexasome and nucleosome in the organization of the DNA around the histone core, which might also be relevant in facilitating transcription through chromatin, as discussed previously (39, 64, 65). Such a stabilized hexasome conformation appears to require physiological ionic strength, as disassembly experiments by increase of ionic strength showed no difference in the dissociation of the H2A·H2B dimers from hexasomes and nucleosomes (66).

Analysis of Histone-DNA Complexes Formed during Assembly by Native PAGE—The different species formed during nucleosome assembly with the DNA_{207} were further examined by native PAGE, which allows the separation of subnucleosomal particles and differently positioned nucleosomes (66–68) (supplemental Fig. S1, C and D). In these experiments the tetrasome was the slowest migrating species followed by the nucleosomes and the faster migrating hexasomes. It can be seen that the amount of tetramer-DNA complex is negligible and well below 10% of the total intensity. Thus, the assembly of tetrasomes into hexasomes takes place quickly, making tetrasomes a rather transient species. In a number of studies the DNA sequence utilized here was shown to harbor multiple nucleosome positions with varying strengths (69–72). From a comparison with recombinant, salt-reconstituted mononucleosomes three major nucleosome bands were identified (supplemental Fig. S1C, NUC_{1-3}), which formed with slightly different kinetics. At least two and possibly three bands (HEX_{1-3}) appeared well before the nucleosome bands, suggesting that these represent the hexasomes, as inferred from the agarose gel analysis.

Kinetic Analysis of Assembly Processes by Fluorescence Anisotropy Measurements—The kinetics of tetrasome and nucleosome assembly were also monitored by fluorescence anisotropy spectroscopy and compared with the EMSA data (Fig. 2). Histone octamer with $H2A^f$ was complexed with NAP1 and then assembled with the DNA template. The course of the reaction was followed by the change in fluorescence anisotropy of $H2A^f$ upon binding to DNA_{207} (Fig. 2*A*) and DNA_{146} (Fig. 2*B*). The anisotropy change was expressed in terms of the fraction of DNA-bound $H2A^f$ and was in good agreement with the EMSA data.

To examine tetrasome formation, assembly reactions were carried out without H2A and H2B, and analyzed by gel electrophoresis and fluorescence anisotropy measurements (Fig. 2, *C* and *D*). These experiments show that the reaction proceeded quickly, given that equilibrium

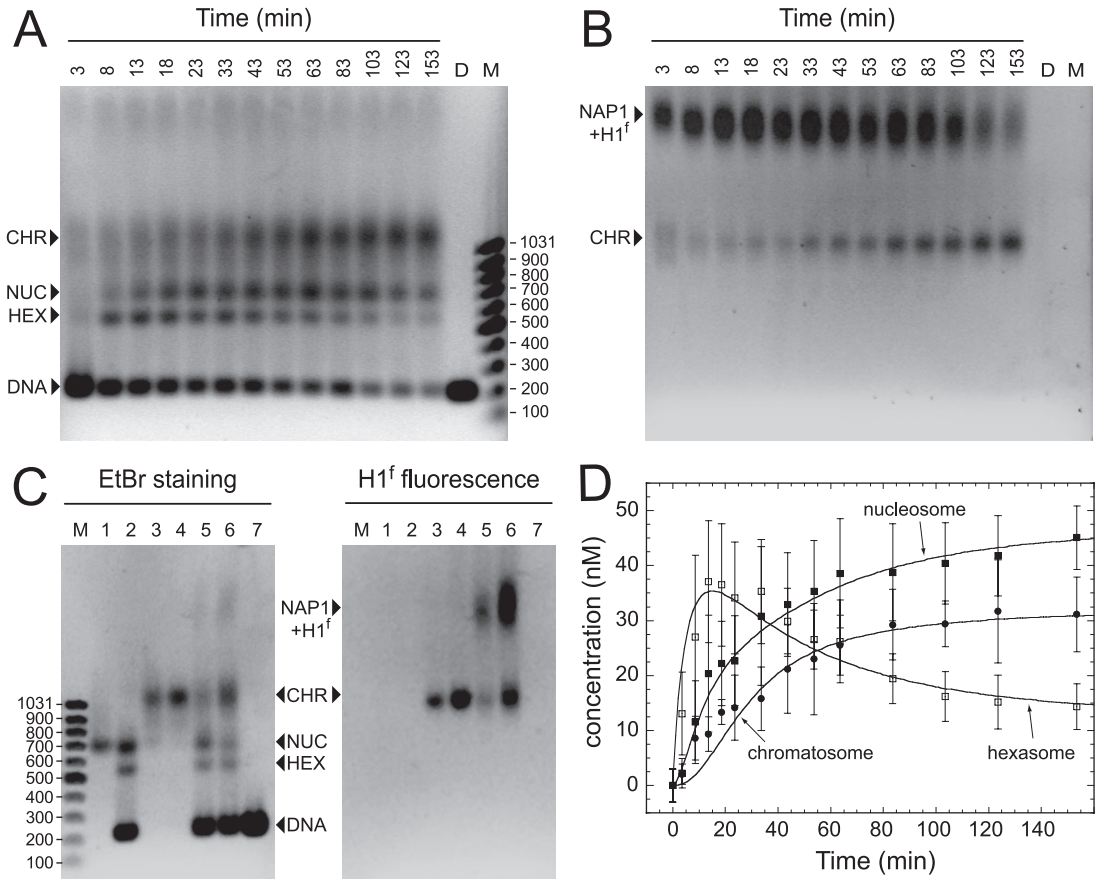

FIGURE 3. **Chromatosome assembly by NAP1 analyzed via agarose gel electrophoresis.** The reaction was carried out with the standard core histone/NAP1 assembly mix and Alexa 488-labeled H1 (*H1^f*) complexed with NAP1. The nucleosome (*NUC*), hexasome (*HEX*), chromatosome (*CHR*), and NAP1$_2$-H1^f complex (*NAP1+H1^f*) bands are indicated. *A*, ethidium bromide staining of one assembly time course. *B*, the fluorescence signal of Alexa 488-labeled H1^f of the gel from *A* is shown. The NAP1-H1 complex and the chromatosome band are visible. *C*, identification of chromatosome particles. *Lane 1*, salt-reconstituted nucleosomes; *lane 2*, NAP1-reconstituted nucleosomes in equilibrium with hexasomes; *lane 3*, salt-reconstituted chromatosomes; *lane 4*, sample of 100 nM salt-reconstituted nucleosomes to which NAP1$_2$-H1^f was added at 100 nM concentration; *lane 5*, end point of NAP1-mediated nucleosome assembly reaction with stoichiometric amount of NAP1$_2$-H1^f; *lane 6*, same as before but with a 3-fold excess of NAP1$_2$-H1^f over nucleosomes; *lane 7*, DNA$_{207}$. *D*, quantification of five assembly kinetics as shown in *A* and *B*. The *solid lines* represent a fit to the models in Equations 1.1, 2.1, 3.1, and 4.1. H1 binding to nucleosomes occurred with a dissociation constant of $K'_{d,4} = 168 \pm 142$ nM (Table 2). Kinetic parameters from the quantitative analysis are given in Table 1.

was reached after ~5 min. The amount of free DNA was significant for both DNA lengths, and only 30–35% of the DNA was complexed into tetrasomes. Hence, the dissociation reaction appeared to be quite prominent and was enhanced by the competition of NAP1 with the DNA for the H3·H4 histones. The resulting data set for tetrasome formation was analyzed according to different models (see below).

The Assembly Mechanism Shows Little Dependence on DNA Sequence—A possible dependence of the assembly reaction on DNA sequence was investigated by the use of templates with random sequences. First, we utilized 146-bp fragments isolated from HeLa cells that were protected from micrococcal nuclease before purification (supplemental Fig. S2A). The kinetics appeared similar to the 5 S rDNA template. In addition, defined fragments of 146 and 207 bp in length with no apparent positioning sequences were studied (supplemental Fig. S2, B and C). The reaction proceeded in a manner similar to experiments with sequences harboring the rDNA positioning motif. Again a difference between the assembly kinetics for the two DNA lengths was observed.

NAP1 Can Guide the Complete Assembly to the Chromatosome Structure—Recent studies highlight the function of NAP1 as a linker histone chaperone (38, 39). To assess the ability of NAP1 to assemble chromatosomes, *e.g.* nucleosomes plus linker histone H1, we utilized fluorescently labeled H1^f. This protein was complexed with NAP1 in the ratio required for stoichiometric binding of one NAP1 dimer per H1 (39). It can be seen in the competition experiment between NAP1 complexes with Alexa 633-labeled H2A^r·H2B dimers and H1^f that the linker histone has a high affinity to NAP1 similar to the H2A·H2B dimer (supplemental Fig. S3).

The NAP1$_2$-H1^f complex was assembled with DNA$_{207}$ together with a core histone/NAP1 premix (Fig. 3). The differential detection of EtBr-stained DNA and the Alexa 488 signal from H1^f in comparison with salt-reconstituted nucleosomes allows the clear identification of the chromatosome particle and demonstrates the incorporation of H1 into the nucleosome structure (Fig. 3, *A–C*). From experiments at different ratios of NAP1$_2$-H1^f to core histones, we infer that H1 binds preferentially to the nucleosome over the hexasome, as the increase of the NAP1$_2$-H1^f concentration primarily reduces the amount of nucleosome (Fig. 3*C*, *lanes 5* and *6*). At stoichiometric ratios of NAP1$_2$-H1^f to nucleosomes, assembly into chromatosomes was not complete, *i.e.* a significant fraction of H1 remained associated with NAP1 (Fig. 3, *A* and *C*). This result was also observed when NAP1$_2$-H1 was added to mononucleosomes preassembled by salt dialysis (data not shown). The later experiments showed that roughly ~75% of nucleosomes bound H1 when equimolar amounts of NAP1$_2$-H1^f (100 nM) were added. This is in accordance with our previous results from extraction experiments on isolated chromatin fibers, which show a substantial removal of H1 by

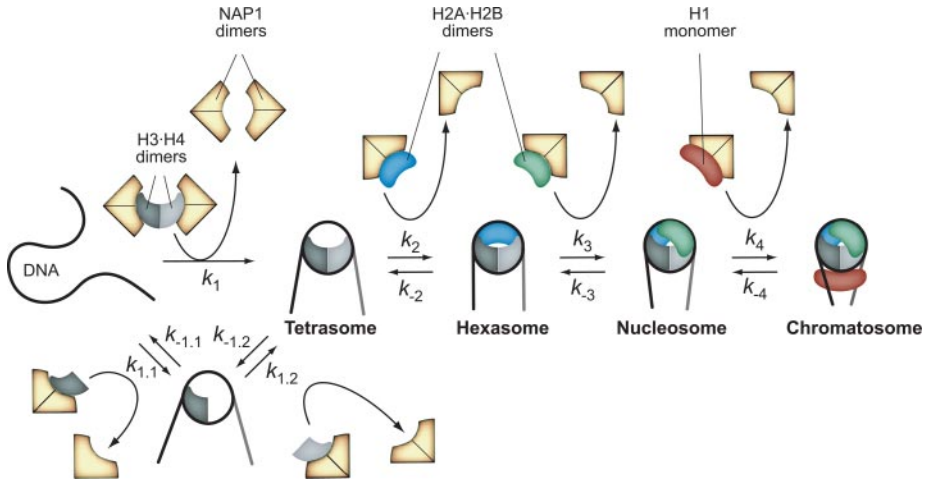

FIGURE 4. **Mechanism of stepwise nucleosome assembly mediated by NAP1.** The reaction is depicted as a process consisting of five reversible reactions with corresponding rate constants. First, two $NAP1_2$-(H3·H4) complexes react consecutively with the DNA to form a tetrasome particle and two free NAP1 dimers. Second, the tetrasome particle reacts with $NAP1_2$-(H2A·H2B) to form a hexasome particle and a NAP1 dimer. Third, the hexasome particle is augmented with a second H2A·H2B dimer from the $NAP1_2$-(H2A·H2B) complex, resulting in a complete nucleosome and release of $NAP1_2$. Fourth, one linker histone is added to the nucleosome from $NAP1_2$-H1. A fit to the depicted model resulted in the values given in Tables 1 and 2. Free NAP1 is present as a dimer under the conditions of the experiment and binds as a dimer to a H3·H4 dimer, a H2A·H2B dimer, or a H1 monomer (36, 39).

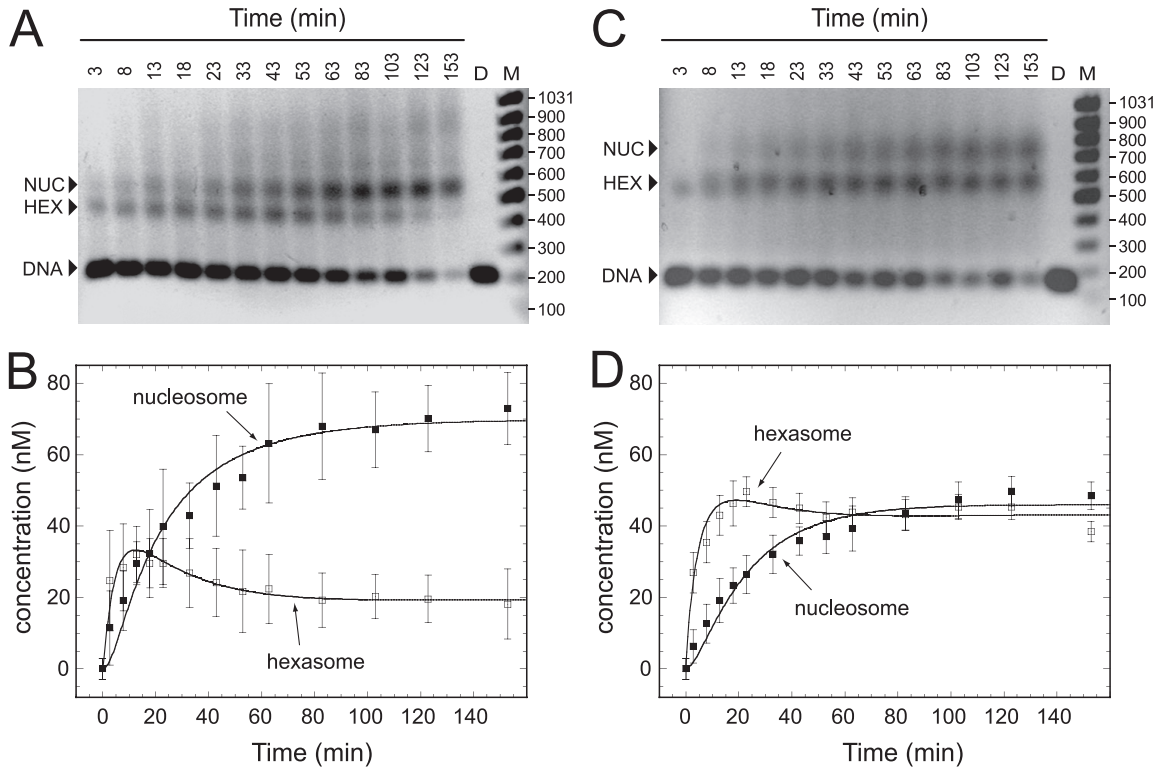

FIGURE 5. **Time course of NAP1-mediated H2A.Z mononucleosome assembly analyzed by agarose gel electrophoresis.** *A*, the assembly kinetics of an H2A.Z-containing octamer with DNA_{207} were investigated. The position of the nucleosome (*NUC*), hexasome (*HEX*), and free DNA_{207} (*DNA*) bands are shown. *Lane D* contains the DNA_{207} sample, and *lane M* is a 100-bp DNA ladder. *B*, for quantification six time courses with DNA_{207} were averaged, and the resulting fractions of nucleosomes (■) and hexasomes (□) are shown. The lines represent a least-squares fit to the model in Equations 1.1–3.1 with the parameters given in Table 1. *C*, same as in *A* but with DNA_{146}. *D*, quantification of 12 time courses with DNA_{146}, with labeling as in *B*.

NAP1 (39). A quantification of the complete chromatosome assembly reaction from several gels is presented in Fig. 3*D*, and the corresponding reaction scheme is given in Fig. 4.

NAP1 Assembles H2A.Z into Mononucleosomes with the Same Mechanism as Canonical H2A—Recent studies report on the interaction of NAP1 with histone octamers containing the variant histone H2A.Z (31, 33). Therefore, it was investigated how NAP1 assembles H2A.Z containing mononucleosomes. Assembly was performed with DNA_{207} (Fig. 5*A*) and DNA_{146} (Fig. 5*C*). The quantification of several gels (Fig. 5, *B* and *D*) revealed that the kinetics and mechanism were similar to the formation of the canonical nucleosome. This result is consistent with previous studies showing that the crystal structure (14) and the solution conformation at physiological ionic strength (73) of nucleosomes containing H2A.Z are similar to the canonical nucleosome. However, the equilibrium between hexasome and nucleosome was shifted somewhat toward the nucleosome with both DNA lengths. This could reflect differences in the stability of the nucleosomal particles that are dependent on the incorporation of the H2A variant and/or differences in their affinity to NAP1. Previous investigations revealed the capability of NAP1 or RNA to disintegrate histone dimers from complete mononucleosomes in a concentration-dependant manner (31, 39, 65). This finding was used to address possible stability differences by performing extraction experiments with salt-reconstituted nucleosomes (canonical and H2A.Z-containing). The H2A.Z nucleosomes were more resistant

to RNA or NAP1-mediated dissociation than the canonical nucleosomes with DNA_{207} (supplemental Fig. S4) as well as with DNA_{146} (data not shown). Thus, the stability difference seems to be mostly intrinsic to the particle and not caused by different affinities to NAP1. An increased stability of H2A.Z nucleosomes was also observed previously in studies on their salt-mediated disassembly (74), whereas in a recent report both H2A.Z- and H2A-containing nucleosomes appear equally resistant to removal by NAP1. The latter result is possibly due to somewhat different experimental conditions that stabilize the nucleosome state (75). The quantitative analysis of our data (see below) indicates that the H2A.Z-containing nucleosomes have an ~3-fold lower dissociation constant. This difference is not pronounced enough to generate an energy-independent, complete exchange of H2A·H2B dimers with H2A.Z·H2B via NAP1, which is in agreement with earlier studies (31). Nevertheless, the higher stability of the H2A.Z·H2B dimer in the nucleosome might contribute to its enrichment in specific types of heterochromatin (76, 77) and its function as a regulatory promoter element (78, 79).

ACF Does Not Change the Kinetics of NAP1-mediated Mononucleosome Formation—In previous experiments clear evidence has been presented that ACF can speed up the assembly of nucleosome arrays with NAP1 as histone carrier (37). Accordingly, two models of the ACF-aided assembly mechanism were proposed (37, 80): One assumes a two-step process in which histone chaperones deposit nucleosomes independently and the remodeling complexes render the irregularly spaced nucleosomes into ordered arrays by translocating single nucleosomes (Ref. 81 and references therein). The second model proposes a cooperative function of chaperones and remodeling complexes during assembly.

To assess the effect of ACF on NAP1-mediated mononucleosome assembly, kinetics were examined in the presence of ACF and 1 mM ATP. In control experiments we noticed that ATP alone affected the kinetics, hindering the hexasome to nucleosome transition, whereas the lowered salt concentration needed for efficient remodeling had little effect (Fig. 6*A*). The modulation caused by ATP could be reproduced with CTP, pointing to a competition of the nucleotides with histone binding to DNA (Fig. 6*A*). A modulating effect of ATP on NAP1-mediated assembly has also been reported previously (37). Apart from this effect, the reactions with ACF proceeded with similar overall kinetics and via the same reaction mechanism as the assembly without the chromatin remodeler and ATP (Fig. 6*B*). From these experiments we concluded that ACF does not increase the rate of NAP1-mediated mononucleosome assembly. The acceleration of the chromatin assembly processes by ACF could rather be established by creating a favorable regular spacing of nucleosomes to form a chromatin fiber in which the packaging of the nucleosomes is optimized and nucleosomes are stabilized. This would disfavor the back-reaction (nucleosome dissociation) and at the same time make more free DNA accessible, facilitating the deposition of additional nucleosomes.

A Kinetic Model for Nucleosome Assembly by NAP1—Based on the results from the gel electrophoretic and fluorescence anisotropy analysis, a kinetic model for the assembly of chromatosomes by NAP1 was derived and is described by Equations 1–4 (Fig. 4). The model is based on the association states of NAP1 alone and its complexes with histones as determined previously (34, 36, 39). NAP1 exists predominantly as a dimeric complex carrying either one H2A·H2B or H3·H4 dimer or a single H1 at the protein concentrations used here. At higher concentrations larger oligomers are observed for complexes with NAP1 (36) as well as for the isolated histones, as reviewed previously (45). The complete reaction scheme is described by Equations 1.1, 2.1, 3.1, and 4.1 and

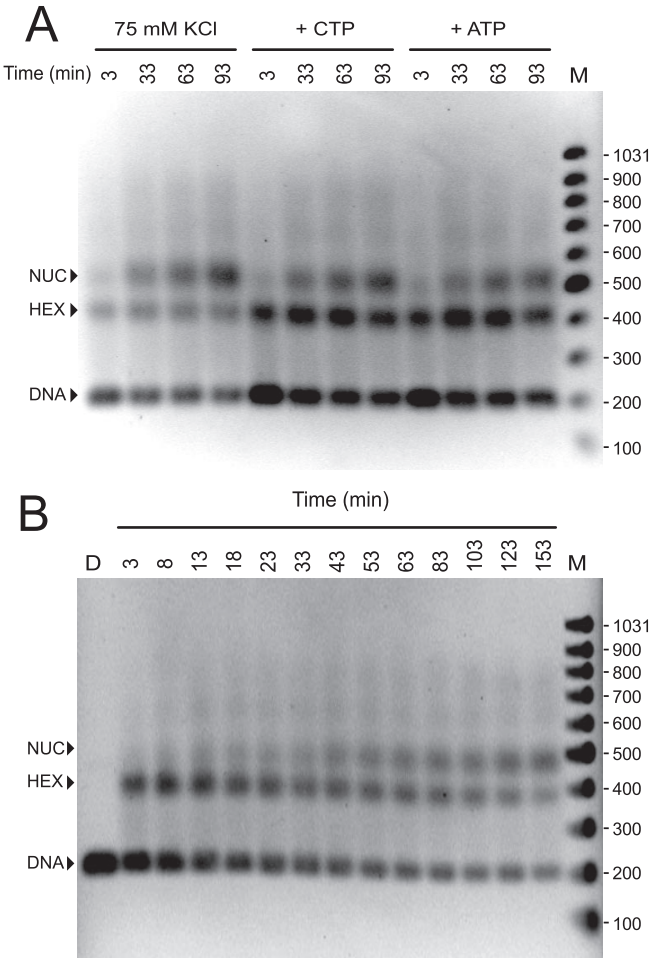

FIGURE 6. **Effect of the activity of the chromatin remodeling complex ACF on the nucleosome assembly reaction.** Labels refer to the nucleosome (*NUC*), hexasome (*HEX*), and free DNA (*DNA*) bands. *A*, assembly kinetics with DNA_{207}. Time points and the presence of either 1 mM CTP or ATP are indicated. A slightly reduced formation of nucleosomes was observed in the presence of either ATP or CTP that was independent of ACF activity. *B*, complete time course (3–153 min) for the assembly reaction with DNA_{207} in the presence of 1 mM ATP and ACF.

was used to derive rate constants from a fit to the EMSA and anisotropy data using the software package GEPASI (61). In these reactions NAP1 mediates the nucleosome assembly reaction without being part of the final product. In this respect NAP1 is similar to an enzymatic component, with the notable difference that it is present in stoichiometric amounts and shifts the equilibrium distribution of species by binding the free histones. If this competitive effect of free $NAP1_2$ is included into apparent rate constants k', the assembly process can be fitted to a simplified set of bimolecular reactions of the form A + B = C. The resulting forward and back rate constants, k', are in units of $M^{-1}\,s^{-1}$ and s^{-1}, with $k'_{forward} = k_{forward}$ and $k'_{back} = (k_{back} \cdot [NAP1_2])$. They yield an apparent equilibrium dissociation constant, $K'_d = k'_{back}/k'_{forward} = (k_{back} \cdot [NAP1_2])/k_{forward} = K_d \cdot [NAP1_2]$. This description, which allows a simple comparison with other protein-DNA binding reactions, is given by Equations 1.2, 2.2, 3.2, and 4.2. The corresponding fit was of similar quality as for the complex model. The resulting rate and equilibrium constants are listed in Tables 1 and 2.

Tetrasome Formation—The rate constants for tetrasome formation were derived from the assembly reactions with only H3·H4 histones by EMSA and anisotropy measurements (Fig. 2, *C* and *D*). Within the resolution of our experiments no smaller subcomplex

TABLE 1

Kinetic rate constants for the NAP1-mediated assembly of nucleosomes

Kinetic rate constants refer to the reactions described in Equations 1 (tetrasome), 2 (hexasome), 3 (nucleosome), and 4 (chromatosome) and were derived from fitting the EMSA and fluorescence anisotropy data with GEPASI (61). Indices of rate constants refer to the corresponding steps where the prime denotes a simplified scheme and in which NAP1 is included only implicitly. See text for details.

Sample	DNA_{207} H2A	DNA_{207} H2A.Z	DNA_{146} H2A	DNA_{146} H2A.Z
$k_1 = k'_1 \approx k_{1.1}$ (M^{-1} s^{-1})		$(2.5 \pm 0.7) \cdot 10^4$		
$k_{-1.2}$ (M^{-1} s^{-1})		$(8.7 \pm 2.6) \cdot 10^3$		
$k'_{-1} \approx k'_{-1.2}$ (s^{-1})		$(3.9 \pm 1.4) \cdot 10^{-3}$		
$k_2 = k'_2$ (M^{-1} s^{-1})		$(4.1 \pm 3.5) \cdot 10^5$		
k_{-2} (M^{-1} s^{-1})		$(4.4 \pm 3.0) \cdot 10^2$		
k'_{-2} (s^{-1})		$(1.9 \pm 1.7) \cdot 10^{-3}$		
$k_3 = k'_3$ (M^{-1} s^{-1})	$(5.9 \pm 0.5) \cdot 10^3$	$(8.8 \pm 0.6) \cdot 10^3$	$(7.3 \pm 1.1) \cdot 10^3$	$(4.5 \pm 0.4) \cdot 10^3$
k_{-3} (M^{-1} s^{-1})	$(0.5 \pm 0.1) \cdot 10^3$	$(0.3 \pm 0.1) \cdot 10^3$	$(4.5 \pm 0.8) \cdot 10^3$	$(0.9 \pm 0.2) \cdot 10^3$
k'_{-3} (s^{-1})	$(2.1 \pm 0.4) \cdot 10^{-4}$	$(1.1 \pm 0.2) \cdot 10^{-4}$	$(13.9 \pm 2.8) \cdot 10^{-4}$	$(3.0 \pm 0.4) \cdot 10^{-4}$
$k_4 = k'_4$ (M^{-1} s^{-1})	$(7.7 \pm 3.7) \cdot 10^3$		ND[a]	
k_{-4} (M^{-1} s^{-1})	$(2.6 \pm 1.2) \cdot 10^3$		ND[a]	
k'_{-4} (s^{-1})	$(1.3 \pm 0.9) \cdot 10^{-3}$		ND[a]	

[a] This parameter could not be determined with DNA_{146}, as chromatosome formation requires a DNA fragment length of about 169 bp or longer. Chromatosome formation with H2A.Z and DNA_{207} showed similar kinetics, but the data set was insufficient to derive reliable values for H1 binding and dissociation.

TABLE 2

Apparent dissociation constants for NAP1-mediated assembly

Equilibrium dissociation constants refer to the reactions described in Equations 1.2, 2.2, 3.2, and 4.2. The value of K'_d is derived from $k'_{back}/k'_{forward}$ (Table 1). As k'_{back} includes the concentration of free $NAP1_2$ the corresponding value of K_d for the complete reactions (Equations 1.1a, 2.1, 3.1, and 4.1) can be obtained from $K'_d = K_d \cdot [NAP1_2]$, where $[NAP1_2]$ is the concentration of free NAP1 dimer.

Sample	$K'_{d,1}$ tetrasome[a]	$K'_{d,2}$ hexasome[b]	$K'_{d,3}$ nucleosome	$K'_{d,4}$ chromatosome
	nM	nM	nM	nM
DNA_{207}, H2A	150 ± 30	4.6 ± 5.7	36 ± 7	168 ± 142[c]
DNA_{207}, H2A.Z	150 ± 30	4.6 ± 5.7	13 ± 2	168 ± 142[c]
DNA_{146}, H2A	150 ± 30	4.6 ± 5.7	190 ± 48	ND[d]
DNA_{146}, H2A.Z	150 ± 30	4.6 ± 5.7	67 ± 11	ND[d]

[a] Average value for the ratio of k'_{-1} to k'_1 (with $k'_{-1} \approx k'_{-1.2}$ and $k_1 = k'_1 \approx k_{1.1}$) determined in the individual assembly experiments with H2A/H2A.Z and DNA_{207}/DNA_{146}. The corresponding value from the kinetic rate constants given in Table 1 is 160 ± 70 nM.

[b] Average value from assembly experiments with H2A/H2A.Z and DNA_{207}/DNA_{146}.

[c] Data are based on the analysis of assembly with the canonical H2A form. The given value corresponds to the complete assembly in the presence of NAP1. A value of $K'_{d,4} = 10 \pm 7$ nM was obtained from binding of 100 nM H1 complexed with 200 nM NAP1 monomer to 100 nM salt-reconstituted nucleosomes. This lower value for $K'_{d,4}$ reflects the reduced $NAP1_2$ concentration of competing free NAP1. Chromatosome assembly with H2A.Z showed similar kinetics and chromatosome/nucleosome ratios as with H2A within the limited number of experiments.

[d] This parameter could not be determined with DNA_{146}, as chromatosome formation requires a DNA fragment length of about 169 bp or longer.

than the tetrasome was detected. Based on earlier results a complex between a H3·H4 dimer and one NAP1 dimer is the predominant association state under the conditions of our experiments (36). Thus, the reaction is likely to occur in two steps, as discussed recently for the *in vivo* process (82–84).

$$NAP1_2(H3 \cdot H4) + DNA \underset{k_{-1.1}}{\overset{k_{1.1}}{\rightleftharpoons}} DNA(H3 \cdot H4) + NAP1_2$$

$$NAP1_2(H3 \cdot H4) + DNA(H3 \cdot H4) \underset{k_{-1.2}}{\overset{k_{1.2}}{\rightleftharpoons}} DNA(H3 \cdot H4)_2 + NAP1_2$$

(Eq. 1.1a)

As the DNA(H3·H4) species is not detected in our experiments, the binding of the two H3·H4 dimers must occur with high cooperativity, *i.e.* $k_{1.2} \gg k_{1.1}$. At higher protein concentrations, where $NAP1_4(H3{\cdot}H4)_2$ is observed (36), the tetrasome will likely form according to Equation 1.1b.

$$NAP1_4(H3 \cdot H4)_2 + DNA \underset{k_{-1}}{\overset{k_1}{\rightleftharpoons}} DNA(H3 \cdot H4)_2 + 2NAP1_2$$

(Eq. 1.1b)

Fitting to the data for tetrasome formation with either Equation 1.1a or 1.1b yielded fits of equally good quality (Fig. 2*D*). The resulting values of $k_{1.1}$ and k_1 were nearly identical, as $k_{1.1}$ was the rate-limiting step for the two-step model with $k_{1.2} \gg k_{1.1}$. It is noted that for fitting the complete nucleosome/chromatosome formation reaction only the total rate of tetrasome formation is relevant for the subsequent reactions. For these it did not make a detectable difference whether Equation 1.1a or 1.1b was selected.

A simplified bimolecular tetrasome formation reaction is given by Equation 1.2, in which NAP1 is not included explicitly. The simplified two-step reaction is given by

$$(H3 \cdot H4) + DNA \underset{k'_{-1.1}}{\overset{k'_{1.1}}{\rightleftharpoons}} DNA(H3 \cdot H4)$$

$$(H3 \cdot H4) + DNA(H3{\cdot}H4) \underset{k'_{-1.2}}{\overset{k'_{1.2}}{\rightleftharpoons}} DNA(H3 \cdot H4)_2$$

(Eq. 1.2a)

The alternative reaction is the tetrasome formation from a preexisting $(H3{\cdot}H4)_2$ tetramer (Equation 1.2b). The latter equation is likely to reflect the appropriate association state of H3·H4 for high protein concentrations (85).

$$(H3 \cdot H4)_2 + DNA \underset{k'_{-1}}{\overset{k'_1}{\rightleftharpoons}} DNA(H3 \cdot H4)_2$$

(Eq. 1.2b)

The rate constants in the above equations are related according to $k_1 = k'_1 \approx k_{1.1}$ and by $k'_{-1.2} = k_{-1.2} \cdot [\mathrm{NAP1_2}] \approx k'_{-1}$. The tetrasome had an apparent dissociation constant of $K'_{d,1} = 150 \pm 30$ nM.

Hexasome Formation—The hexasome formation is characterized by its rapid formation from the tetrasome, reducing the tetrasome concentration below the detection limit in our experiments.

$$\mathrm{DNA(H3 \cdot H4)_2} + \mathrm{NAP1_2(H2A \cdot H2B)} \underset{k_{-2}}{\overset{k_2}{\rightleftharpoons}} \mathrm{DNA(H3 \cdot H4)_2(H2A \cdot H2B)} + \mathrm{NAP1_2} \quad \text{(Eq. 2.1)}$$

The corresponding simplified reaction is given by Equation 2.2 with $k'_2 = k_2$ and $k'_{-2} = k_2 \cdot [\mathrm{NAP1_2}]$.

$$\mathrm{DNA(H3 \cdot H4)_2} + \mathrm{(H2A \cdot H2B)} \underset{k'_{-2}}{\overset{k'_2}{\rightleftharpoons}} \mathrm{DNA(H3 \cdot H4)_2(H2A \cdot H2B)} \quad \text{(Eq. 2.2)}$$

The apparent dissociation constant for the hexasome formation was 4.6 ± 5.7 nM. Thus, the hexasome is a stable intermediate that forms during nucleosome assembly in the presence of the competing factor NAP1. This is also reflected by the presence of hexasomal particles at the end of the time courses, where equilibrium was reached.

Nucleosome Formation—The assembly of the nucleosome is completed by addition of the second H2A·H2B dimer according to Equations 3.1 and 3.2 for the simplified reaction ($k'_3 = k_3$ and $k'_{-3} = [\mathrm{NAP1_2}] \cdot k_{-3}$).

$$\mathrm{DNA(H3 \cdot H4)_2(H2A \cdot H2B)} + \mathrm{NAP1_2(H2A \cdot H2B)} \underset{k_{-3}}{\overset{k_3}{\rightleftharpoons}} \mathrm{DNA(H3 \cdot H4)_2(H2A \cdot H2B)_2} + \mathrm{NAP1_2} \quad \text{(Eq. 3.1)}$$

$$\mathrm{DNA(H3 \cdot H4)_2(H2A \cdot H2B)} + \mathrm{(H2A \cdot H2B)} \underset{k'_{-3}}{\overset{k'_3}{\rightleftharpoons}} \mathrm{DNA(H3 \cdot H4)_2(H2A \cdot H2B)_2} \quad \text{(Eq. 3.2)}$$

The DNA length and the substitution of canonical H2A with H2A.Z significantly influenced the resulting dissociation constant of this reaction. The reduced presence of hexasomes for the H2A.Z-containing particles can be assigned to a ~3-fold lower dissociation constant of the H2A.Z nucleosome (Table 2). When the shorter DNA was used, the apparent $K'_{d,3}$ increased around 5-fold from 31 ± 7 to 190 ± 48 nM for the canonical nucleosome and from 13 ± 2 to 67 ± 11 nM for the H2A.Z nucleosome. This difference appears to be caused mostly by alterations in the dissociation rate of the nucleosome, which varied more significantly then the association rate (Table 1).

Chromatosome Formation—The complete chromatosome structure is obtained by augmentation of nucleosomes with H1.

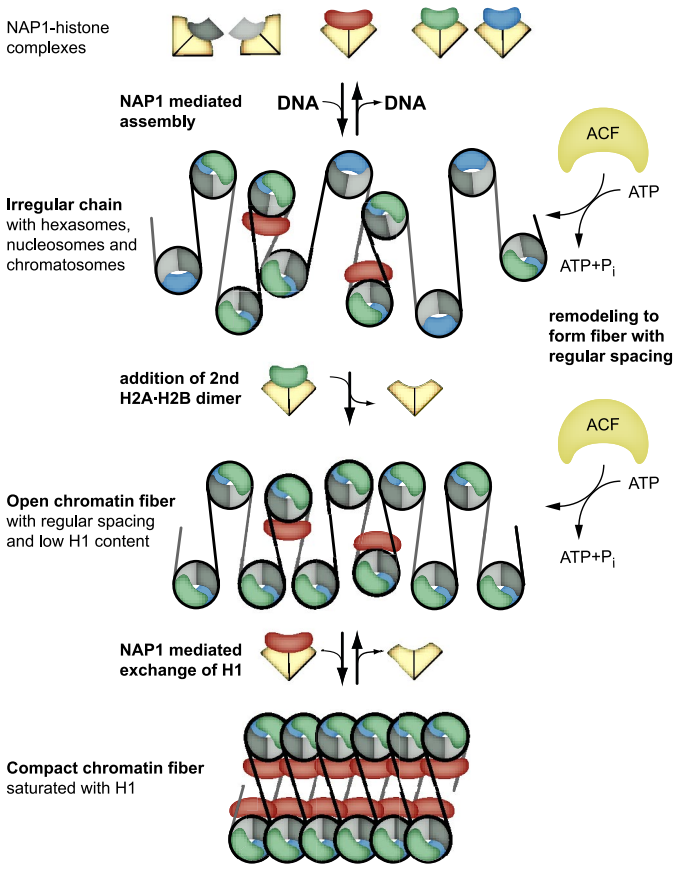

FIGURE 7. **Model for the folding of the chromatin fiber in the presence of NAP1 and a remodeler/assembly factor like ACF.** The deposition of (sub)nucleosomal particles by NAP1 and other chaperones results in formation of a dynamic unordered chromatin chain that contains hexasomes, nucleosomes, and chromatosomes with irregular spacing on the DNA. This chain is converted into a regular structure by ATP-dependent remodeling machines such as ACF. In this conformation a chromatin fiber is established in which the nucleosomes are stabilized. Thus, H2A·H2B dimer dissociation is impaired, and the hexasome state is depleted. In contrast, NAP1-mediated binding and dissociation of linker histone is still possible. The ratio of $\mathrm{NAP1_2}$-H1 to nucleosomes will determine the linker histone content (Fig. 3). Free NAP1 is able to extract H1 from chromatin fibers and induce a transition from a compact chromatin state with high linker histone content to a more open conformation (39).

$$\mathrm{DNA(H3 \cdot H4)_2(H2A \cdot H2B)_2} + \mathrm{NAP1_2H1} \underset{k_{-4}}{\overset{k_4}{\rightleftharpoons}} \mathrm{DNA(H3 \cdot H4)_2(H2A \cdot H2B)_2H1} + \mathrm{NAP1_2} \quad \text{(Eq. 4.1)}$$

The simplified reaction is described by Equation 4.2, with $k'_4 = k_4$ and $k'_{-4} = [\mathrm{NAP1_2}] \cdot k_{-4}$.

$$\mathrm{DNA(H3 \cdot H4)_2(H2A \cdot H2B)_2} + \mathrm{H1} \underset{k'_{-4}}{\overset{k'_4}{\rightleftharpoons}} \mathrm{DNA(H3 \cdot H4)_2(H2A \cdot H2B)_2H1} \quad \text{(Eq. 4.2)}$$

The apparent $K'_{d,4}$ for complete assembly by NAP1 in the presence of 150 nM $\mathrm{NAP1_2}$-H1 was calculated from k'_4 and k'_{-4} to be 169 ± 142 nM. A value of $K'_{d,4} = 10 \pm 7$ nM was derived by binding of 100 nM $\mathrm{NAP1_2}$-H1 to the same concentration of preassembled, salt-reconstituted nucleosomes on $\mathrm{DNA_{207}}$ (data not shown). This increase of the

apparent affinity reflects the shift of the equilibrium with decreasing amounts of NAP1. It is consistent with a previously determined dissociation constant for H1 nucleosome binding of about 2 nM in the absence of chaperones (86).

Comparison with in Vivo Assembly Kinetics—Previously it was shown that H3 and H4 are bound in the sub-minute time scale to DNA *in vivo*, whereas the deposition of H2A and H2B takes 2–10 min (40). We estimate from experiments with autofluorescent histones (87–89) that the equivalent of 1–10 μM histone octamer is not bound to the DNA and available for assembly during replication. At these μM concentrations, the assembly of a mononucleosome would occur with $t_{1/2} \sim 1$ min or even faster in the minimal system studied here, making the kinetics comparable with those observed *in vivo*.

Conclusions—NAP1 is capable of guiding the complete and specific assembly of core, variant, and linker histones with DNA into nucleosomes and chromatosomes (Fig. 4). It reliably prevents unspecific histone aggregation as well as the formation of DNA-(H2A·H2B) complexes that cannot maturate into nucleosomes (31, 38, 80). The specific formation of the nucleosome/chromatosome complex can be explained simply on the basis of thermodynamic differences in the interactions among NAP1, histones, and DNA. The affinity of NAP1 toward H3·H4 appears to be approximately that of linear DNA, thus causing a transfer of H3·H4 onto DNA. In contrast, the relative affinity of H2A·H2B toward the chaperone must be above that for DNA, which prevents release of H2A·H2B onto free DNA. Once a tetrasome structure is formed, it provides a higher affinity binding platform for H2A·H2B dimers so that the hexasome and nucleosome particles form. The latter structure is the preferred binding site for association with the linker histone so that the complete chromatosome complex assembles readily in a specific manner.

Our results have a number of implications for the assembly of the chromatin fiber, as proposed by the model depicted in Fig. 7. First, the presence of a hexameric histone structure as a stable assembly intermediate, as well as the rapid equilibrium between the nucleosome and the chromatosome species, suggests that all three species will be present simultaneously to form the nascent chromatin fiber with an irregular spacing of these particles. Second, the activity of the chromatin remodeler ACF has no effect on the assembly of the mononucleosome but will be required to form a more regular chromatin fiber structure. Third, the equilibrium between hexasomes and nucleosomes is shifted toward the nucleosome as the final chromatin fiber conformation with regular spacing of nucleosomes is established. In this higher order structure, core histones are protected from possible extraction by NAP1 through internucleosomal contacts. In contrast, the relative affinity of NAP1 to H1 is high enough to modulate its content in the fiber structure without disintegration of core nucleosomes (39).

Acknowledgments—We are grateful to Katalin Fejes Tóth for helpful discussions, and we thank Gernot Längst for the ACF sample, Leica Microsystems and Irmgard Sinning for access to instruments, and Tom Owen-Hughes, Karolin Luger, and Timothy Richmond for plasmid vectors.

REFERENCES

1. Luger, K., Mäder, A. W., Richmond, R. K., Sargent, D. F., and Richmond, T. J. (1997) *Nature* **389,** 251–260
2. Verreault, A. (2000) *Genes Dev.* **14,** 1430–1438
3. Tyler, J. K. (2002) *Eur. J. Biochem.* **269,** 2268–2274
4. Akey, C. W., and Luger, K. (2003) *Curr. Opin. Struct. Biol.* **13,** 6–14
5. Zlatanova, J., Leuba, S. H., and van Holde, K. (1998) *Biophys. J.* **74,** 2554–2566
6. Zlatanova, J., Leuba, S. H., and van Holde, K. (1999) *Crit. Rev. Eukaryotic Gene Expression* **9,** 245–255
7. Weintraub, H., and Groudine, M. (1976) *Science* **193,** 848–856
8. Annunziato, A. T., and Seale, R. L. (1984) *Nucleic Acids Res.* **12,** 6179–6196
9. Jackson, V., and Chalkley, R. (1985) *Biochemistry* **24,** 6930–6938
10. Jackson, V. (1990) *Biochemistry* **29,** 719–731
11. Krude, T. (1999) *Eur. J. Biochem.* **263,** 1–5
12. Ahmad, K., and Henikoff, S. (2002) *Mol. Cell* **9,** 1191–1200
13. Janicki, S. M., Tsukamoto, T., Salghetti, S. E., Tansey, W. P., Sachidanandam, R., Prasanth, K. V., Ried, T., Shav-Tal, Y., Bertrand, E., Singer, R. H., and Spector, D. L. (2004) *Cell* **116,** 683–698
14. Fan, J. Y., Gordon, F., Luger, K., Hansen, J. C., and Tremethick, D. J. (2002) *Nat. Struct. Biol.* **9,** 172–176
15. Dryhurst, D., Thambirajah, A. A., and Ausio, J. (2004) *Biochem. Cell Biol.* **82,** 490–497
16. Thiriet, C., and Hayes, J. J. (2005) *Genes Dev.* **19,** 677–682
17. Haushalter, K. A., and Kadonaga, J. T. (2003) *Nat. Rev. Mol. Cell Biol.* **4,** 613–620
18. Daban, J. R., and Cantor, C. R. (1982) *J. Mol. Biol.* **156,** 771–789
19. Daban, J. R., and Cantor, C. R. (1982) *J. Mol. Biol.* **156,** 749–769
20. Smith, S., and Stillman, B. (1989) *Cell* **58,** 15–25
21. Bonner, W. M. (1975) *J. Cell Biol.* **64,** 431–437
22. Kleinschmidt, J. A., Dingwall, C., Maier, G., and Franke, W. W. (1986) *EMBO J.* **5,** 3547–3552
23. Laskey, R. A., Honda, B. M., Mills, A. D., and Finch, J. T. (1978) *Nature* **275,** 416–420
24. Prado, A., Ramos, I., Frehlick, L. J., Muga, A., and Ausio, J. (2004) *Biochem. Cell Biol.* **82,** 437–445
25. Arnan, C., Saperas, N., Prieto, C., Chiva, M., and Ausio, J. (2003) *J. Biol. Chem.* **278,** 31319–31324
26. Sherwood, P. W., and Osley, M. A. (1991) *Genetics* **128,** 729–738
27. Ray-Gallet, D., Quivy, J. P., Scamps, C., Martini, E. M., Lipinski, M., and Almouzni, G. (2002) *Mol. Cell* **9,** 1091–1100
28. Ishimi, Y., Hirosumi, J., Sato, W., Sugasawa, K., Yokota, S., Hanaoka, F., and Yamada, M. (1984) *Eur. J. Biochem.* **142,** 431–439
29. Ito, T., Bulger, M., Kobayashi, R., and Kadonaga, J. T. (1996) *Mol. Cell. Biol.* **16,** 3112–3124
30. Loyola, A., and Almouzni, G. (2004) *Biochim. Biophys. Acta* **1677,** 3–11
31. Park, Y. J., Chodaparambil, J. V., Bao, Y., McBryant, S. J., and Luger, K. (2005) *J. Biol. Chem.* **280,** 1817–1825
32. McQuibban, G. A., Commisso-Cappelli, C. N., and Lewis, P. N. (1998) *J. Biol. Chem.* **273,** 6582–6590
33. Mizuguchi, G., Shen, X., Landry, J., Wu, W. H., Sen, S., and Wu, C. (2004) *Science* **303,** 343–348
34. Park, Y. J., and Luger, K. (2006) *Proc. Natl. Acad. Sci. U. S. A.* **103,** 1248–1253
35. McBryant, S. J., Park, Y. J., Abernathy, S. M., Laybourn, P. J., Nyborg, J. K., and Luger, K. (2003) *J. Biol. Chem.* **278,** 44574–44583
36. Fejes Tóth, K. F., Mazurkiewicz, J., and Rippe, K. (2005) *J. Biol. Chem.* **280,** 15690–15699
37. Ito, T., Bulger, M., Pazin, M. J., Kobayashi, R., and Kadonaga, J. T. (1997) *Cell* **90,** 145–155
38. Shintomi, K., Iwabuchi, M., Saeki, H., Ura, K., Kishimoto, T., and Ohsumi, K. (2005) *Proc. Natl. Acad. Sci. U. S. A.* **102,** 8210–8215
39. Kepert, J. F., Mazurkiewicz, J., Heuvelman, G. L., Fejes Toth, K., and Rippe, K. (2005) *J. Biol. Chem.* **280,** 34063–34072
40. Worcel, A., Han, S., and Wong, M. L. (1978) *Cell* **15,** 969–977
41. Jackson, V. (1987) *Biochemistry* **26,** 2315–2325
42. Jackson, V. (1988) *Biochemistry* **27,** 2109–2120
43. Senshu, T., Fukuda, M., and Ohashi, M. (1978) *J. Biochem.* (*Tokyo*) **84,** 985–988
44. Cremisi, C., and Yaniv, M. (1980) *Biochem. Biophys. Res. Commun.* **92,** 1117–1123
45. van Holde, K. E. (1989) *Chromatin*, pp. 241–256, Springer, Heidelberg, Germany
46. Smith, S., and Stillman, B. (1991) *EMBO J.* **10,** 971–980
47. Ladoux, B., Quivy, J. P., Doyle, P., Roure, O., Almouzni, G., and Viovy, J. L. (2000) *Proc. Natl. Acad. Sci. U. S. A.* **97,** 14251–14256
48. Wagner, G., Bancaud, A., Quivy, J. P., Clapier, C., Almouzni, G., and Viovy, J. L. (2005) *Biophys. J.* 3647–3659
49. Kleinschmidt, J. A., Seiter, A., and Zentgraf, H. (1990) *EMBO J.* **9,** 1309–1318
50. Ruiz-Carrillo, A., Jorcano, J. L., Eder, G., and Lurz, R. (1979) *Proc. Natl. Acad. Sci. U. S. A.* **76,** 3284–3288
51. Tatchell, K., and Van Holde, K. E. (1977) *Biochemistry* **16,** 5295–5303
52. Wilhelm, F. X., Wilhelm, M. L., Erard, M., and Duane, M. P. (1978) *Nucleic Acids Res.* **5,** 505–521
53. Jorcano, J. L., and Ruiz-Carrillo, A. (1979) *Biochemistry* **18,** 768–774
54. Hansen, J. C., van Holde, K. E., and Lohr, D. (1991) *J. Biol. Chem.* **266,** 4276–4282
55. Camerini-Otero, R. D., Sollner-Webb, B., and Felsenfeld, G. (1976) *Cell* **8,** 333–347
56. Luger, K., Rechsteiner, T. J., and Richmond, T. J. (1999) *Methods Mol. Biol.* **119,** 1–16
57. Luger, K., Rechsteiner, T. J., Flaus, A. J., Waye, M. M., and Richmond, T. J. (1997) *J. Mol. Biol.* **272,** 301–311
58. Bruno, M., Flaus, A., Stockdale, C., Rencurel, C., Ferreira, H., and Owen-Hughes, T. (2003) *Mol. Cell* **12,** 1599–1606

59. Richmond, T. J., Searles, M. A., and Simpson, R. T. (1988) *J. Mol. Biol.* **199,** 161–170
60. Simpson, R. T., Thoma, F., and Brubaker, J. M. (1985) *Cell* **42,** 799–808
61. Mendes, P. (1993) *Comput. Appl. Biosci.* **9,** 563–571
62. Vogel, S. K., Schulz, A., and Rippe, K. (2002) *Nucleic Acids Res.* **30,** 4094–4101
63. Lakowicz, J. R. (1999) *Principles of Fluorescence Spectroscopy*, pp. 308–309, Kluwer Academic/Plenum Publishers, New York
64. Kireeva, M. L., Walter, W., Tchernajenko, V., Bondarenko, V., Kashlev, M., and Studitsky, V. M. (2002) *Mol. Cell* **9,** 541–552
65. Levchenko, V., and Jackson, V. (2004) *Biochemistry* **43,** 2359–2372
66. Levchenko, V., Jackson, B., and Jackson, V. (2005) *Biochemistry* **44,** 5357–5372
67. Pennings, S. (1997) *Methods* (*Amst.*) **12,** 20–27
68. Pennings, S. (1999) *Methods Enzymol.* **304,** 298–312
69. Simpson, R. T., and Stafford, D. W. (1983) *Proc. Natl. Acad. Sci. U. S. A.* **80,** 51–55
70. Dong, F., Hansen, J. C., and van Holde, K. E. (1990) *Proc. Natl. Acad. Sci. U. S. A.* **87,** 5724–5728
71. Yodh, J. G., Woodbury, N., Shlyakhtenko, L. S., Lyubchenko, Y. L., and Lohr, D. (2002) *Biochemistry* **41,** 3565–3574
72. Pennings, S., Meersseman, G., and Bradbury, E. M. (1991) *J. Mol. Biol.* **220,** 101–110
73. Abbott, D. W., Ivanova, V. S., Wang, X., Bonner, W. M., and Ausio, J. (2001) *J. Biol. Chem.* **276,** 41945–41949
74. Park, Y. J., Dyer, P. N., Tremethick, D. J., and Luger, K. (2004) *J. Biol. Chem.*
75. Okuwaki, M., Kato, K., Shimahara, H., Tate, S., and Nagata, K. (2005) *Mol. Cell. Biol.* **25,** 10639–10651
76. Rangasamy, D., Berven, L., Ridgway, P., and Tremethick, D. J. (2003) *EMBO J.* **22,** 1599–1607
77. Rangasamy, D., Greaves, I., and Tremethick, D. J. (2004) *Nat. Struct. Mol. Biol.* **11,** 650–655
78. Farris, S. D., Rubio, E. D., Moon, J. J., Gombert, W. M., Nelson, B. H., and Krumm, A. (2005) *J. Biol. Chem.* **280,** 25298–25303
79. Guillemette, B., Bataille, A. R., Gevry, N., Adam, M., Blanchette, M., Robert, F., and Gaudreau, L. (2005) *PLoS Biol.* **3,** e384
80. Nakagawa, T., Bulger, M., Muramatsu, M., and Ito, T. (2001) *J. Biol. Chem.* **276,** 27384–27391
81. Strohner, R., Wachsmuth, M., Dachauer, K., Mazurkiewicz, J., Hochstatter, J., Rippe, K., and Langst, G. (2005) *Nat. Struct. Mol. Biol.* **12,** 683–690
82. Tagami, H., Ray-Gallet, D., Almouzni, G., and Nakatani, Y. (2004) *Cell* **116,** 51–61
83. Annunziato, A. T. (2005) *J. Biol. Chem.* **280,** 12065–12068
84. English, C. M., Maluf, N. K., Tripet, B., Churchill, M. E., and Tyler, J. K. (2005) *Biochemistry* **44,** 13673–13682
85. Baxevanis, A. D., Godfrey, J. E., and Moudrianakis, E. N. (1991) *Biochemistry* **30,** 8817–8823
86. Nightingale, K., Dimitrov, S., Reeves, R., and Wolffe, A. P. (1996) *EMBO J.* **15,** 548–561
87. Kimura, H., and Cook, P. R. (2001) *J. Cell Biol.* **153,** 1341–1353
88. Weidemann, T., Wachsmuth, M., Knoch, T. A., Muller, G., Waldeck, W., and Langowski, J. (2003) *J. Mol. Biol.* **334,** 229–240
89. Fejes Tóth, K. F., Knoch, T. A., Wachsmuth, M., Frank-Stohr, M., Stohr, M., Bacher, C. P., Muller, G., and Rippe, K. (2004) *J. Cell Sci.* **117,** 4277–4287 k

Supplementary Figure S1. Electrophoretic mobility of (sub)nucleosomal particles on agarose and polyacrylamide gels. (A+B) Lanes 1-3: complexes with canonical histones; lanes 4-6: complexes with H2A.Z histone instead of H2A; lanes 1 and 4: salt reconstituted mononucleosomes; lanes 2 and 5: NAP1 assembled nucleosomes and hexasomes; lanes 3 and 6: NAP1 assembled tetrasomes; lane M: 100 bp DNA ladder. The positions of nucleosome (NUC), hexasome (HEX) and tetrasomes (TET) are indicated and mobility patterns were analyzed on (A) DNA_{207} or (B) DNA_{146}. (C) Time course of NAP1 mediated mononucleosome assembly with DNA_{207} analyzed by native PAGE. Lanes marked 3-123 min show samples taken from different time points during the reconstitution reaction. Lane "T" contains the reconstituted tetrasome and "M" the DNA standard. The positions of tetramer (TET), three major nucleosome (NUC_1, NUC_2 and NUC_3), two or three hexasome (HEX_1/HEX_2, HEX_3) and the free DNA_{207} band are indicated. (D) Intensity profiles of the 3 and 123 min time points.

Supplementary Figure S2. Time course of NAP1 mediated mononucleosome assembly on random DNA sequences that do not contain a defined nucleosome positioning sequence. The observed kinetics were similar to those observed for the rDNA positioning sequences of the same length. The nucleosome (NUC), and hexasome (HEX) and free DNA (DNA) band are labeled. The lanes marked with "D" and "M" contain the input DNA and the length standard. (A) Assembly reaction with a pool of 146 bp DNA fragments extracted from HeLa cells. (B) Assembly with a defined non-positioning sequence of 146 bp produced by PCR. (C) Assembly with a defined non-positioning sequence of 207 bp produced by PCR. A reduced formation of (sub)nucleosomal particles was observed compared to the 146 bp DNA shown in panel B as observed also for the rDNA fragments DNA_{207} and DNA_{146} (Fig. 1).

Supplementary Figure S3. Competitive binding of Alexa 633 labeled $H2A^r$·H2B dimer (red) and Alexa 488 labeled $H1^f$ (green) to NAP1. A saturated complex of $NAP1_2$-($H2A^r$·H2B) dimer (4 μM NAP1 dimer with 2 μM $H2A^r$·H2B dimer), lane 1, was titrated with increasing amounts of $H1^f$ (lanes 2-6: addition $H1^f$ to a concentration of 0.2, 0.4, 0.6, 0.8 and 1.4 μM). It can be see that $H1^f$ replaces some of the NAP1 bound $H2A^r$·H2B dimer leading to the formation of a $NAP1_2$-$H1^f$ complex with green color that comigrates with the red NAP1-($H2A^r$·H2B) complex. This results in a yellow fluorescence signal of the band. Lane 7: complex of $NAP1_2$-$H1^f$ (4 μM NAP1 monomer with 2 μM $H1^f$). The partial substitution of $H2A^r$·H2B dimer from the NAP1 complex with $H1^f$ at stoichiometric concentrations indicates comparable binding affinities of both proteins to the $NAP1_2$ dimer. The indicated association states of NAP1-histone complexes are based on previous measurements (36,39).

Supplementary Figure S4. Disassembly of nucleosomes into hexasomes induced by the addition of NAP1 or RNA. Canonical or H2A.Z containing nucleosomes reconstituted by salt dialysis on DNA_{207} at a concentration of 100 nM were incubated with increasing amounts of NAP1 (0.5, 3, 5 µM) or HeLa total RNA (7.5, 18, 58 ng/μl) for three hours at 25 °C. The position of nucleosomes, (NUC), hexasomes (HEX), free DNA (DNA) as well as the two major rRNAs (RNA_1 and RNA_2) are indicated. For both types of nucleosomes an increase of the hexasome fraction with added competitor is seen. However, the effect was reduced for the H2A.Z containing nucleosomes indicating an increased stability of the nucleosome formed with this variant histone.

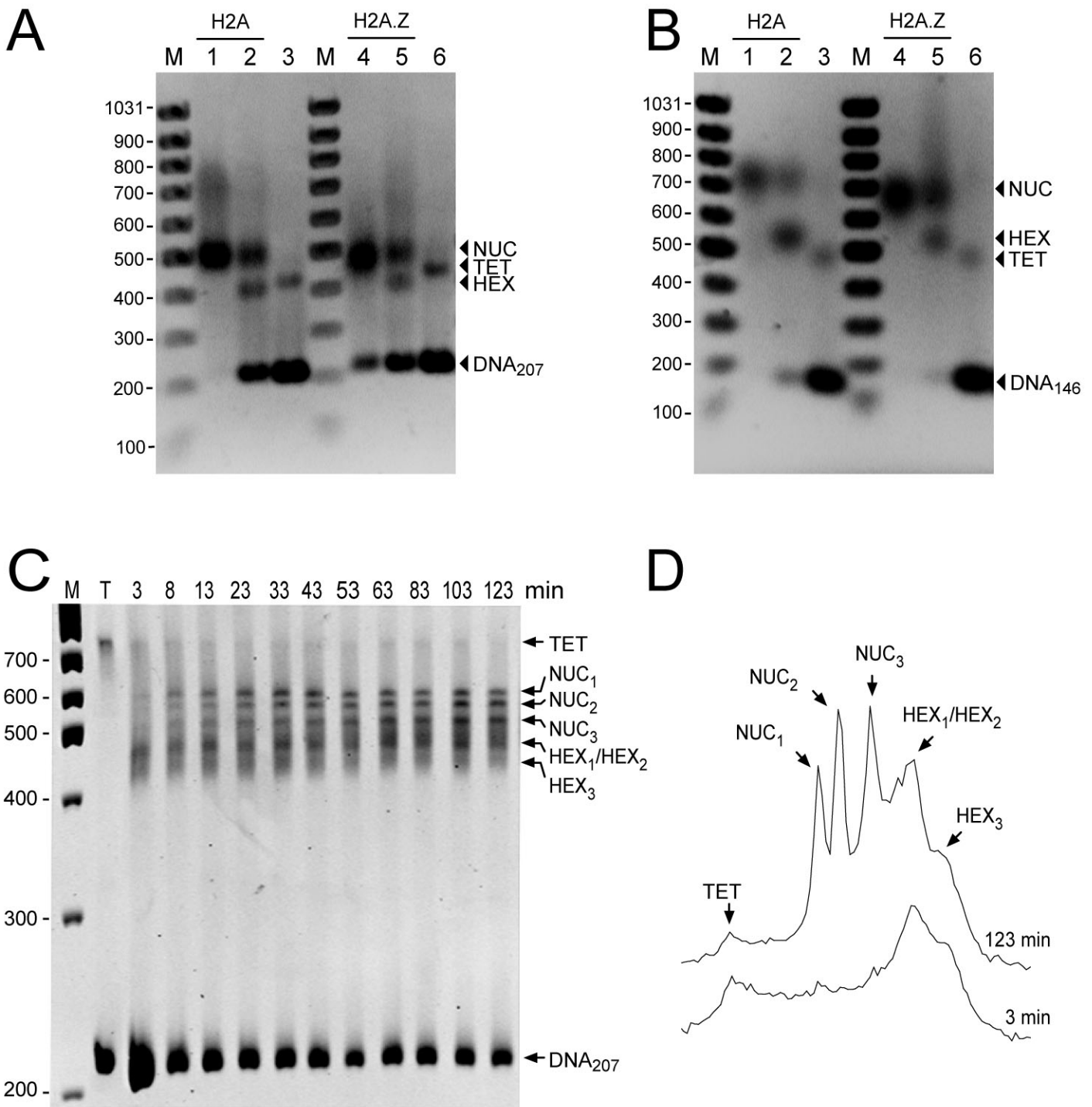

Mazurkiewicz et al. Supplementary Fig. S1

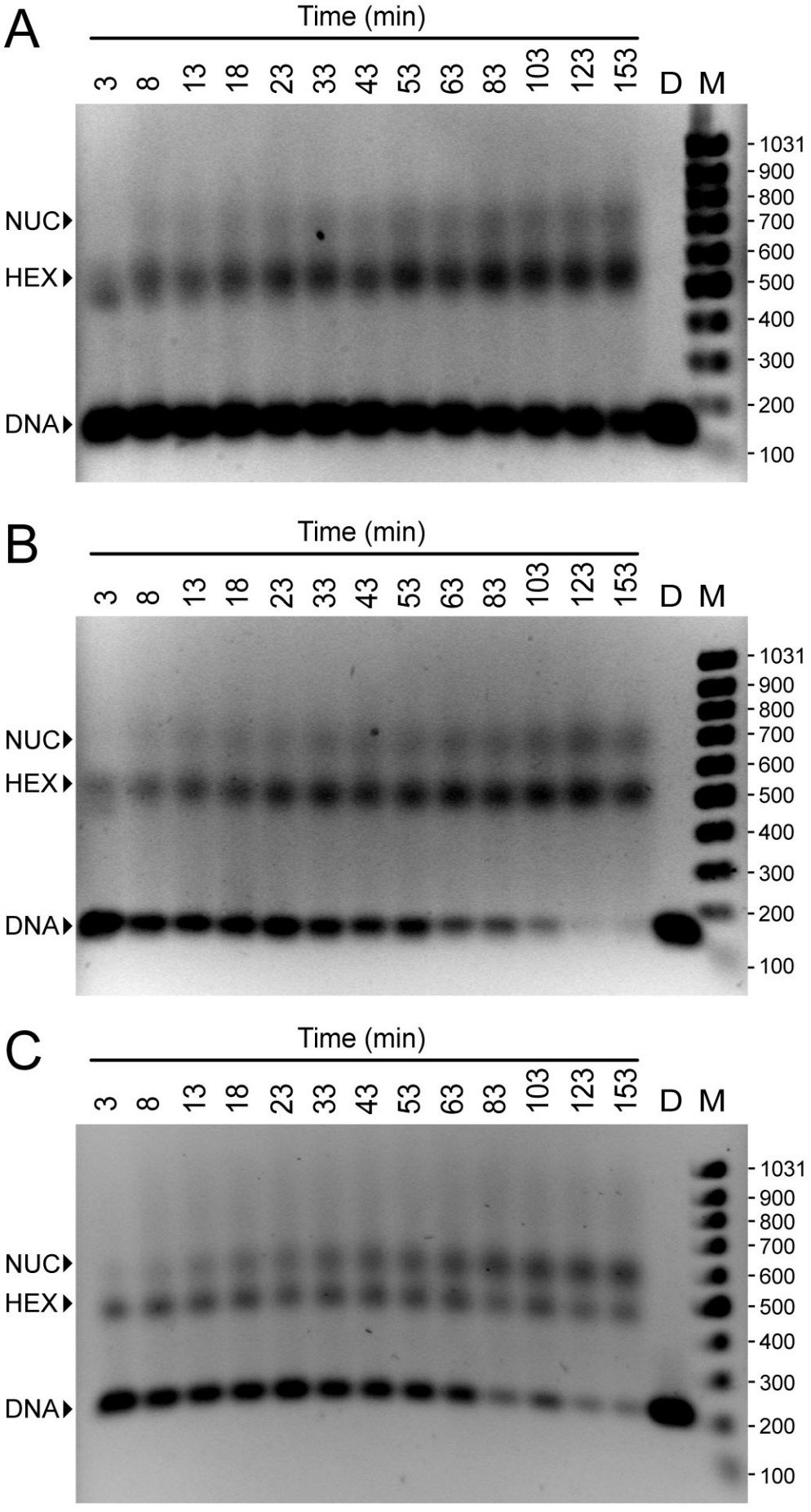

Mazurkiewicz et al. Supplementary Fig. S2

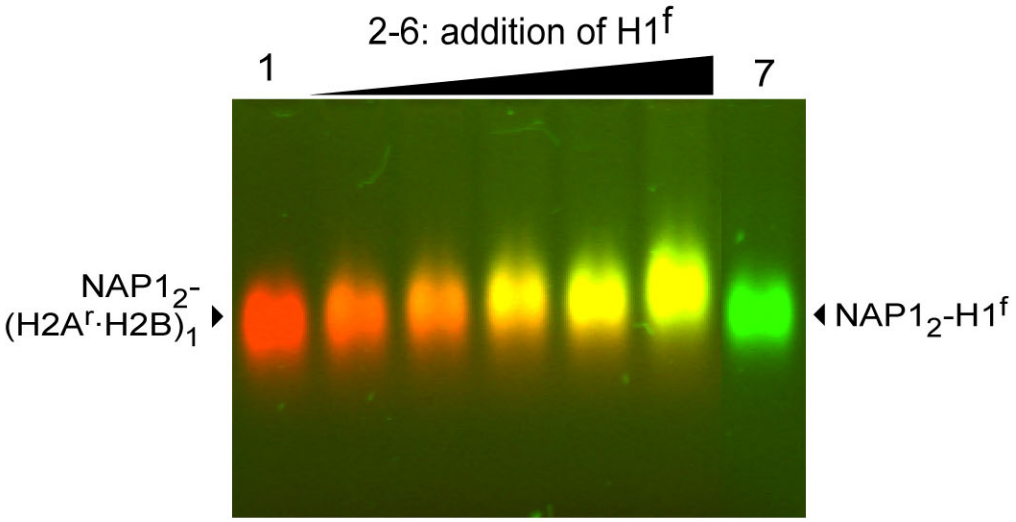

Mazurkiewicz et al. Supplementary Fig. S3

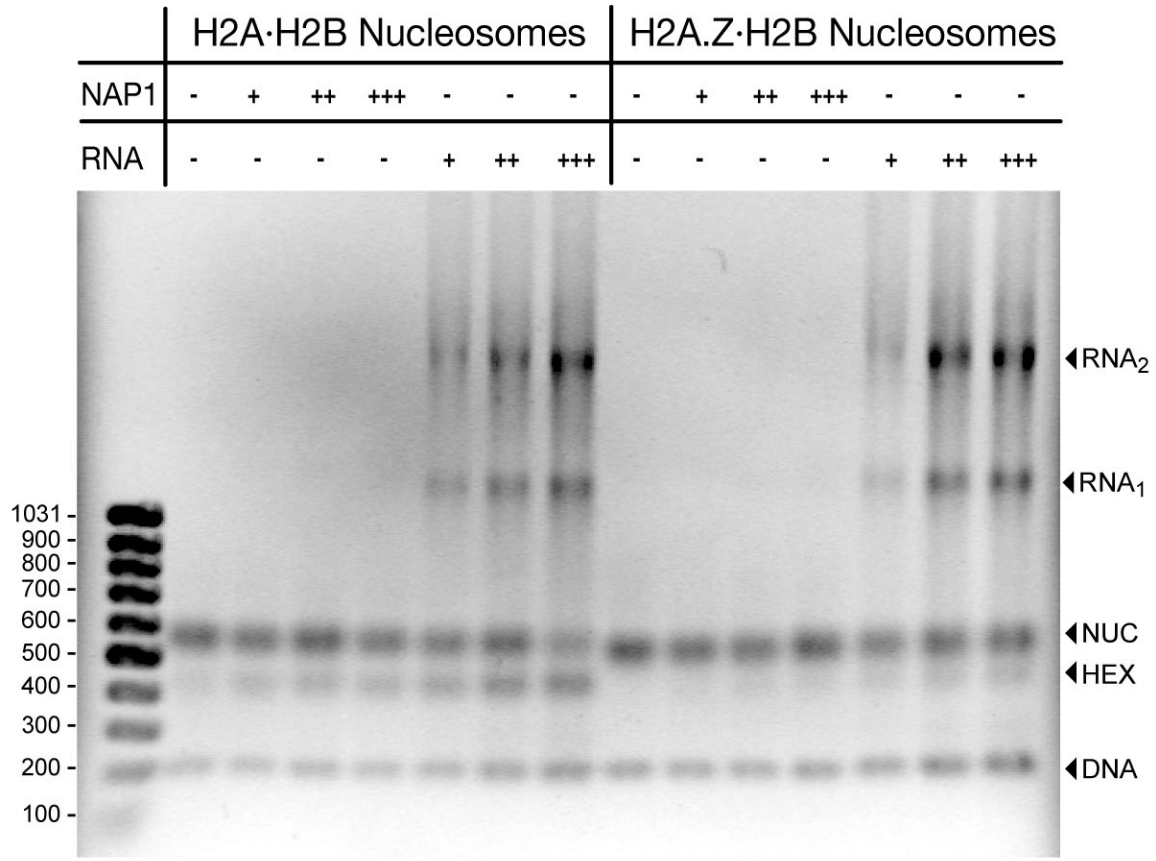

Mazurkiewicz et al. Supplementary Fig. S4